

# Grazing instabilities and post-bifurcation behavior in an impacting string

K. D. Murphy and T. M. Morrison

Department of Mechanical Engineering, University of Connecticut, Storrs, Connecticut 06269-3139

(Received 27 June 2001; revised 21 October 2001; accepted 13 November 2001)

A theoretical and experimental investigation of the nonlinear dynamic response of a periodically excited string subject to a knife-edge amplitude restraint is presented. The amplitude restraint creates an impact condition as the amplitude of the response grows. The focus of this work is on the influence of a grazing instability; this zero-velocity impact event leads to complicated, post-bifurcation behavior ranging from multifrequency, periodic motion to chaos. In addition to looking at the response numerically, parameter combinations leading to an incidence of grazing are clearly identified in the excitation force excitation frequency parameter space using a multiple scales perturbation analysis. Modeling issues, numerical difficulties, and experimental limitations are also discussed. © 2002 Acoustical Society of America. [DOI: 10.1121/1.1433806]

PACS numbers: 43.40.Cw [ANN]

## I. INTRODUCTION

A wide variety of problems in science and engineering involve impact events. Some simple examples include engine valve closure, gears experiencing backlash, a moored ship bumping into a dock, a pendulum contacting an amplitude restraint, and a ball bouncing on a table, see Refs. 1–4. The principle feature of these *impact oscillators* is that there is a discontinuity in the stiffness at the onset of contact. This highly nonlinear contact event is at the heart of the diverse response characteristics previously reported.

Many studies of impacting systems have involved discrete, single degree-of-freedom (DOF) models and have shown a host of complicated behavior including period doubling bifurcations, quasiperiodicity, high-period impacting orbitals, and, of course, chaos. For the sake of numerically computing the response of these single DOF systems, a two model approach, shown in Fig. 1, is commonly taken. In the free-play region [Fig. 1(b)], the standard 1 DOF linear oscillator is used. At the moment of impact ( $x = \sigma$ ), the equation of motion switches to the two spring model shown on the right-hand side of Fig. 1(c). As contact is achieved and lost between the mass and the wall, the governing equations are toggled between these two single DOF models.

Early exceptions to studying low-dimensional, single DOF systems have considered the motion of a continuous beam subject to amplitude constraints at the tip.<sup>5–8</sup> However, even these models are 1 DOF in nature, since the beam is discretized using a single mode Galerkin projection (resulting in a single ordinary differential equation). In the free-play region, a cantilevered shape function is used in the discretization. In the contact region, a clamped–pinned shape function is used. So, once again, the solution is found by switching between two governing ODE's as contact is initiated and lost.

More recently, solitary wave solutions have been investigated for a piecewise linear beam model.<sup>9</sup> This particular analysis did not involve a single mode discretization of the governing equation and rendered two generic solution types.

The present work takes a theoretical, numerical, and ex-

perimental approach to examine the response of a tensioned string subject to harmonic excitation and a knife edge amplitude restraint. Practical realizations of an impacting string system include moving textile threadlines, the fiber optic cable drawing process, and wire electro-discharge machining. The idealized system under consideration is shown schematically in Fig. 2. The principle objectives of this study are (i) to identify parameter combinations which lead to the zero-velocity grazing instability<sup>10,11</sup> and (ii) to examine the post-bifurcation behavior of the system.

## II. EQUATIONS OF MOTION

To begin, the string is assumed to be a homogeneous, 1D elastic continuum. The knife-edge amplitude constraint is modeled as a localized, stiff spring which is set off from the equilibrium position of the string by a distance  $\sigma$ . In this case, the strain energy per unit length of the system may be expressed as

$$U = \int_0^L \left[ \frac{1}{2} EA \epsilon^2 + \frac{1}{2} K \delta(x - x_r) (v(x) - \sigma)^2 \right] dx, \quad (1)$$

where  $\epsilon = u_{,x} + v_{,x}^2/2 + P/EA$  is the axial strain,  $u$  and  $v$  are the axial and transverse deflections, respectively,  $E$  is the elastic modulus,  $A$  is the cross-sectional area of the string,  $P$  is the applied axial tension,  $L$  is the length of the string,  $\delta$  is the Dirac delta function, and  $x_r$  is the location of the restraint. The discontinuous restraint stiffness is given by

$$K = \begin{cases} 0 & -\infty < v(x_r) < \sigma, \\ \text{Large} & \sigma \leq v(x_r) < \infty. \end{cases} \quad (2)$$

The kinetic energy of the system is

$$T = \frac{1}{2} \int_0^L m [v_{,t}^2 + u_{,t}^2] dx, \quad (3)$$

where  $m$  is the mass per unit length. Finally, the work done on the string by the externally applied force is

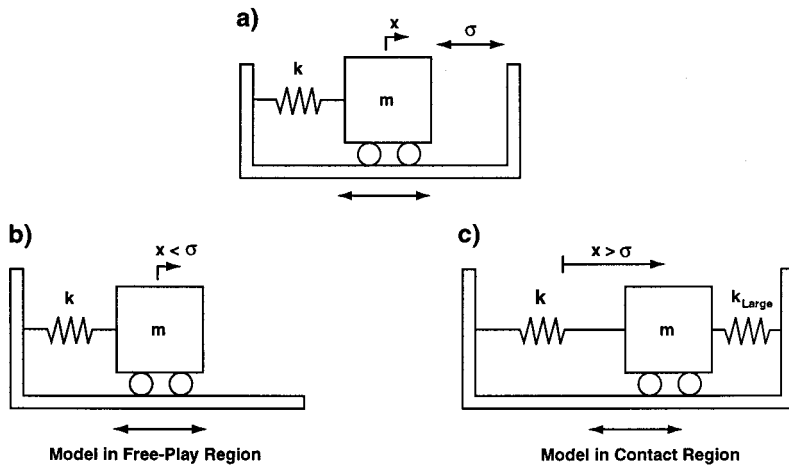


FIG. 1. A schematic of a common single degree-of-freedom model for impact problems.

$$W = \int_0^L F \sin(\omega t) \delta(x - x_0) v(x) dx, \quad (4)$$

where  $F$  is the excitation amplitude,  $\omega$  is the excitation frequency, and  $x_0$  is the point of application of the force.

Using these expressions in Hamilton's principle leads to two partial differential equations of motion governing the axial and transverse motion of the string. To further simplify matters, the axial motion of the string is assumed to take place quasistatically. This assumption is justified since our attention will be focused near the first transverse resonant frequency, which is typically much lower than the first axial frequency. With this quasistatic stretching assumption, the transverse equation of motion for the string is

$$mv_{,tt} + cv_{,t} - \left[ \int_0^{L1} \frac{EA}{2L} v_{,x}^2 dx + P \right] v_{,xx} + K \delta(x - x_r)(v(x) - \sigma) = F \sin(\omega t) \delta(x - x_0). \quad (5)$$

Viscous structural damping, given by  $cv_{,t}$ , has been added to capture the dissipative nature of the system. It should also be noted that, with the exception of the amplitude restraint stiffness, this equation is identical to the nonlinear string model developed from a Newtonian point-of-view by Narasimha.<sup>12</sup> This equation is recast in nondimensional form

$$V_{,\tau\tau} + 2\zeta\omega_1 V_{,\tau} - \left[ \int_0^1 \frac{EA}{2P\pi^2} V_{,\xi}^2 d\xi + \frac{1}{\pi^2} \right] V_{,\xi\xi} + \frac{KL^2}{P\pi^2} \delta(\xi - \xi_r)(V(\xi) - \bar{\sigma}) = \frac{\delta(\xi - \xi_0)}{P\pi^2} F \sin(\Omega\tau), \quad (6)$$

where the displacement is  $V = v/L$ , the axial coordinate is  $\xi = x/L$ , the gap size is  $\bar{\sigma} = \sigma/L$ ,  $\zeta$  is the damping ratio,  $\Omega = \omega/\omega_1$  is the nondimensional forcing frequency, and time is rescaled to  $\tau = t\sqrt{P\pi^2/mL^2}$ . This equation is discretized spatially using a Galerkin procedure along with the expansion

$$V(\xi, \tau) = \sum_{j=1}^n a_j(\tau) \sin(j\pi\xi). \quad (7)$$

The  $i$ th equation of motion, resulting from that procedure, is

$$\ddot{a}_i + 2\zeta\omega_1 \dot{a}_i + \left[ \frac{EA}{P} \sum_{j=1}^n \frac{(j\pi)^4}{4} a_j^2 + i^2 \right] a_i + \frac{KL^2}{P\pi^2} \left[ \sum_{j=1}^n a_j \sin(j\pi\xi_r) - \bar{\sigma} \right] \sin(i\pi\xi_r) = \frac{2 \sin(i\pi\xi_0)}{\pi^2} \frac{F}{P} \sin(\Omega\tau). \quad (8)$$

Nonlinearities arise in this equation from two sources: (i) geometric nonlinearities associated with large deflections and (ii) the restraint stiffness  $K$ , as defined by Eq. (2). Also, note that the  $i$ th linear natural frequency is  $\omega_i = \sqrt{i^2 P \pi^2 / mL^2}$  rad/s and that time has been rescaled with the first natural frequency.

### III. NUMERICAL SIMULATION

In the impacting regime, numerical solutions to Eq. (8) will be sought. However, before proceeding, it is important to ensure that reliable solutions are obtained. There are four primary challenges to obtaining such solutions. The first stems from the large stiffness discontinuity which occurs at impact; the governing equations [Eq. (8)] often become numerically stiff at impact, meaning that the eigenvalues of the local Jacobian matrix range over several orders of magni-

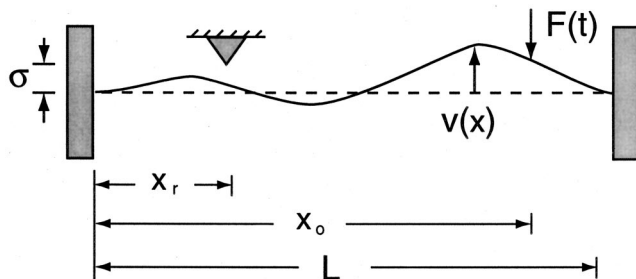


FIG. 2. An overhead schematic of the vibrating string system, including the knife-edge amplitude restraint and periodic excitation  $F(t)$ .

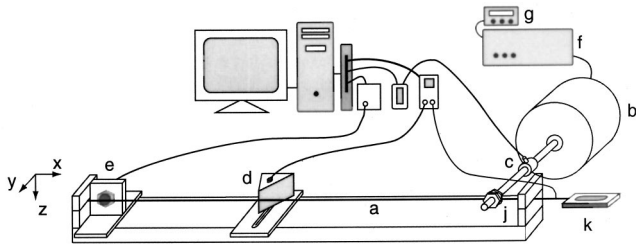


FIG. 3. A diagram of the components comprising the experimental setup.

tude. To remedy this problem, an adaptive step, hybrid integration routine is used. This routine uses Geer's method during nonstiff portions of the solution and automatically switches to a backwards difference method, which is slower but extremely stable, during the stiff portions. Second, it is crucial to determine the exact moment of impact, since this will have a tremendous influence on the computed response. However, it is also computationally inefficient to use an extremely small time step throughout the simulation. To overcome this difficulty, the equations of motion are recast as described by Henon.<sup>13</sup> In this new form, the instant of impact is easily determined without having to resort to an extremely small time step. Third, due to the finite expansion of the displacement field in Eq. (7), the issue of modal convergence arises. Typically, 20 terms ( $n=20$ ) were retained; the addition of more terms did not change the qualitative character of the response or the parameter values associated with the observed bifurcations. The final challenge involves the transient dynamics. Transient oscillations, induced at the start of impacting, die slowly in this lightly damped system. In all cases presented, 250 forcing cycles are allowed to elapse before the response is considered to be at steady state.

## IV. EXPERIMENTAL STUDY

### A. Experimental system

A schematic of the experimental setup is shown in Fig. 3. It consists of a tensioned bass guitar string (a), an electro-mechanical shaker (b), a force transducer (c), a knife-edge constraint (d), and a displacement sensor (e). The shaker was driven by a power amplifier (f) and a wave form generator (g). This system also employed a control system that helped maintain a constant forcing amplitude, even during large amplitude deflections of the string.

The sinusoidal force was provided by an electromechanical shaker in the  $y$  direction, such that motion occurred in the  $(x,y)$  plane. A lightweight aluminum stinger was attached to the shaker armature and used to deliver the periodic force to the string. The threaded end of the stinger was connected to the string by means of two nuts, which were sinched down to pinch the wire (j). A PCB force transducer was attached to the stinger to monitor the force supplied by the shaker. The data acquisition software was able to monitor the amplitude of the applied load to two decimal places. However, distortions in the *shape* of the wave form, occurring during impacts, could not be monitored quantitatively. Fortunately, the onset of these distortions were dramatic and easily identifiable.

The impact condition was realized by a wedge-shaped aluminum block (d). The block was mounted to a fixture that allowed the wedge location to be moved (varying  $\xi_r$ ) and the gap separation to be changed (varying  $\bar{\sigma}$ ).

The planar displacement of the string was monitored using a noncontacting displacement sensor (e). The sensor produced a voltage proportional to the displacement of the wire from its equilibrium position. Because the sensor can only detect small motion, it was mounted at  $\xi=0.035$ , where the motion was expected to be small.

The string was made of a solid wire core of diameter 0.31 mm. Wire windings around this core increased the net string diameter to 2.31 mm. Because the inner core was primarily responsible for sustaining the axial tension (the windings are expected to take up very little of the axial load), the axial rigidity  $EA$  was calculated using only the inner core area. An axial tension of  $P=45$  N was applied by mounting the left end of the string and using a spring scale (k) to deliver the load to the right end. With this load applied, the right end was clamped down.

The parameters of the system under consideration include the string length  $L=0.6$  m; the load applied at  $\xi_0=0.933$ ; the knife-edge restraint located at  $\xi_r=0.3$ ; the displacement sensor at the right end of the string at  $\xi_s=0.035$ . The wire has a Young's modulus of  $E=205 \times 10^3$  MPa and a mass per unit length of  $m=0.02095$  kg/m<sup>2</sup>. Using the log-dec method, the damping ratio was found to be  $\zeta=0.005$ . Under these conditions, the fundamental linear natural frequency is  $\omega_1=38.6$  Hz.

### B. Experimental procedure

There were two experimental goals. The first was to determine the nonimpacting amplitude-frequency response diagram. This would validate the governing equations in the freeplay region. The second goal involved measuring the parameter combinations of the forcing amplitude and driving frequency ( $F, \omega$ ) that led to the initiation of impacts. The procedures for obtaining the necessary data are outlined below.

For the first series of tests, the system was setup as described in the preceding section, but with the knife-edge restraint removed. A sinusoidal excitation was applied to the wire and the frequency was swept in order to determine experimentally the natural frequency. Having completed this, the excitation frequency was then set at 40% of the first natural frequency. The system was driven at this frequency for approximately 30 s to ensure transients had decayed. The voltage from the displacement sensor was then read by a LabVIEW data acquisition program, which recorded the peak-to-peak displacement of the string at the sensor. The excitation frequency was incremented by 1 Hz and the procedure was carried out again. This process was continued until the frequency reached approximately  $\Omega=1.4$ . In an attempt to capture any dramatic hysteresis, the entire procedure was repeated, starting at a frequency of  $\Omega=1.4$  and gradually decreasing through resonance.

The second series of tests involved predicting the parameter combinations ( $F, \omega$ ) that correspond to the transition from no-impact to impact. To accomplish this, the displace-

ment sensor was removed and the knife-edge amplitude restraint was attached to the system. The positive terminal of a DC power supply was attached to the right end of the string, which was hanging through the end support (see Fig. 3). The negative terminal of that same power supply was connected to a light bulb, which was also in electrical contact with the amplitude restraint. If the vibration caused the string to contact the restraint, the circuit would be completed and the light would blink. This closed circuit was also connected to the LabVIEW software, which recorded the first incidence of contact. To develop the required parameter plot, the frequency was fixed and the forcing amplitude was increased (quasistatically) until contact was detected. The force was turned down and the frequency was incremented. After transients died out, the force was gradually increased again until contact was detected. Repeating this process, gives the required parameter diagram.

## V. PARAMETER STUDY—INITIATION OF GRAZING

Consider gradually increasing the excitation frequency from a small value. As the first natural frequency is approached, the response amplitude at  $\xi_r$  will grow until it eventually equals the gap separation  $\bar{\sigma}$ . At the peak of this motion, the string *grazes* the knife edge. This zero velocity impact can lead to a variety of post-grazing responses as the frequency is increased; this will be demonstrated in Sec. VI. As a result, it would prove useful to know *a priori* what combinations of the forcing amplitude and frequency lead to grazing.

Grazing occurs when the response amplitude at  $\xi_r$  equals to the gap distance  $\bar{\sigma}$ . These parameter combinations are found using two methods: (i) a linear analysis for small gap separations where the response amplitude need not be large for impact and (ii) a multiple scales perturbation analysis for moderate gap separations, where the motion is weakly nonlinear.

### A. Linear motion

If it is assumed that the displacement is less than one diameter,  $\bar{\sigma} < \mathcal{O}(d)$ , it is reasonably safe to assume that the motion is nearly linear. For simplicity, it is also assumed that only one mode (the  $i$ th) participates. Under these assumptions, the nonlinear terms are eliminated from Eq. (8) and only the  $i$ th equation of motion remains. Letting the amplitude  $|V(\xi_r)|$  equal  $\bar{\sigma}$  gives the grazing condition

$$\frac{2 \sin(i\pi\xi_r)}{\pi^2} \frac{F}{P} = \frac{\bar{\sigma}}{\sin(i\pi\xi_r)} \sqrt{[i^2 - \Omega^2]^2 + [2\zeta\Omega]^2}. \quad (9)$$

It is important to recognize that the actual deflection of the string is made up of the sum of all of the modes. Hence, this one-mode-at-a-time approach does not give a completely accurate picture of the motion, since modes may sum constructively or destructively at different locations. Nonetheless, near the  $i$ th resonant frequency, these results should prove satisfactory since the  $i$ th mode will dominate the response.

## B. Nonlinear motion: A perturbation analysis

The method of multiple time scales is used to obtain the response amplitude of the string in the free-play region. Again, a single mode approach is taken. The analysis presented here is limited to first nonlinear order, though higher order solutions could easily be found. To begin, the equation of motion is rescaled. Specifically, the modal amplitude is recast as  $a_i = \epsilon^{1/2} A_i$  which leads to

$$\ddot{A}_i + \beta \dot{A}_i + i^2 A_i + k \epsilon A_i^3 = \epsilon^{-1/2} \mathcal{F} \sin(\Omega \tau), \quad (10)$$

where  $\epsilon$  is a small positive parameter,  $\beta$  is a damping coefficient,

$$\mathcal{F} = \frac{2 \sin(i\pi\xi_r)}{\pi^2} \frac{F}{P}$$

is a nondimensional forcing amplitude [see Eqs. (8) and (9)], and

$$k = \frac{EA}{P} \frac{(i\pi)^4}{4}$$

is the coefficient to the cubic nonlinearity [see Eq. (8)]. Two new time scales are also introduced,

$$T_n = \epsilon^n \Omega \tau, \quad n = 0, 1. \quad (11)$$

$T_0$  is the fast time scale and  $T_1$  is a slow time scale that captures the effects of damping, nonlinearity, and the external excitation. Derivative operators on the original time scale  $\tau$  may be expressed in terms of the derivatives on the new time scales as

$$\frac{d}{d\tau} = \Omega(D_0 + \epsilon D_1 + \dots), \quad (12)$$

$$\frac{d^2}{d\tau^2} = \Omega^2(D_0^2 + 2\epsilon D_0 D_1 + \dots), \quad (13)$$

where  $D_i$  is a derivative operator on the  $i$ th time scale. Next, the rescaled modal amplitude is expressed to first nonlinear order as a uniform expansion in the new time scales,

$$A_i = \sum_{n=0}^1 \epsilon^n \alpha_n(T_0, T_1). \quad (14)$$

The excitation amplitude and the damping coefficients are intentionally reordered so that they will appear at the first nonlinear order:  $F = \epsilon^{3/2} F_1$  and  $\Omega\beta = \epsilon\beta_1$ . Finally, only excitation frequencies near the  $i$ th nondimensional natural frequency are considered. In other words,

$$\Omega^2 = i^2 + \epsilon\sigma_1, \quad (15)$$

where  $\sigma_1$  represents the amount of detuning from the  $i$ th resonant frequency. These definitions are substituted into the discretized equation of motion, Eq. (10), and collected into groups with like powers of  $\epsilon$ . The linear order equation,  $\mathcal{O}(\epsilon^0)$ , is

$$D_0^2 \alpha_0 + \alpha_0 = 0. \quad (16)$$

The solution to Eq. (16) is

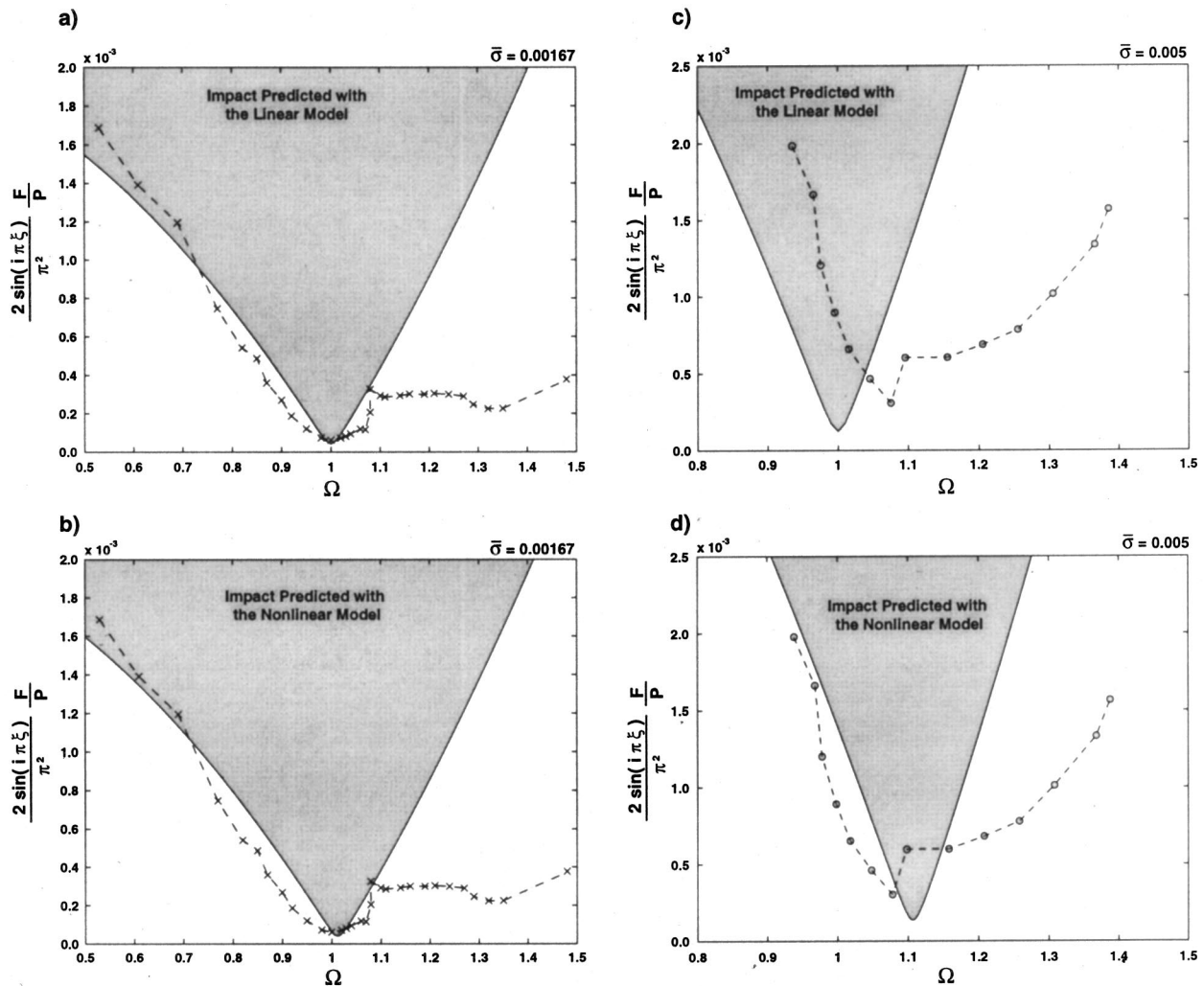


FIG. 4. Parameter combinations leading to the initiation of impacting motion. (a) and (b) Correspond to a small gap size  $\bar{\sigma}=0.00167$  (linear and nonlinear, respectively), while (c) and (d) correspond to a larger gap size  $\bar{\sigma}=0.005$  (linear and nonlinear, respectively).

$$\alpha_0 = C_0(T_1)e^{j\omega t} + \bar{C}_0(T_1)e^{-j\omega t}, \quad (17)$$

where  $j = \sqrt{-1}$  is the imaginary number and the overbar denotes the complex conjugate. The unknown coefficient,  $C_0$ , is a slowly varying complex amplitude which will be determined at the next order. The first nonlinear order equation,  $\mathcal{O}(\epsilon)$ , is

$$D_0^2 \alpha_1 + \alpha_1 = \frac{1}{i^2} \left[ -\beta_1 D_0 \alpha_0 - 2i^2 D_1 D_0 \alpha_0 - k \alpha_0^3 - \sigma_1 D_0^2 \alpha_0 + \frac{F_1}{2} (e^{iT_0} + e^{-iT_0}) \right]. \quad (18)$$

Substituting  $\alpha_0$ , as given in Eq. (17), into the right-hand side of Eq. (18) enables a solution for  $\alpha_1$ . However, there are terms on the right-hand side that are proportional to  $e^{\pm jT_0}$ , creating a resonance condition for  $\alpha_1$ . To ensure that  $\alpha_1$  remains bounded, these *secular* terms are set to zero. This procedure yields

$$-\beta_1 j C_a - 2i^2 j D_1 C_a - 3k C_a^2 C_a + \sigma_1 C_a + \frac{1}{2} F_1 = 0. \quad (19)$$

For steady motion, the derivative on the  $T_1$  time scale is zero:  $D_1 C_a = 0$ . Also, because  $C_a$  is complex, it may be expressed in polar form as  $C_a = \frac{1}{2} M e^{j\phi}$ . Substituting this expression into the secular equation renders two algebraic equations (arising from the real and imaginary parts of the equation) for the amplitude  $M$  and the phase  $\phi$ :

$$-\Omega \beta M - F \sin(\phi) = 0, \quad (20)$$

$$-\frac{3}{4} k M^3 + (\Omega^2 - i^2) M + F \cos(\phi) = 0. \quad (21)$$

These nonlinear algebraic equations may be solved using a Newton-Raphson solution technique.

These equations may be used in two ways. First, by prescribing the forcing frequency and amplitude, the response may be determined ( $M$  and  $\phi$ ). Alternatively, the frequency and amplitude may be specified (i.e.,  $M$  could be set equal to  $\bar{\sigma}$ ), and the necessary force could be determined. It is the second approach which will be used to develop the desired parameter diagrams.

### C. Parameter study—Results

Figures 4(a) and (b) show the parameter combinations that lead to impact for a separation of  $\bar{\sigma}=0.00167$  ( $\sigma=1.0$

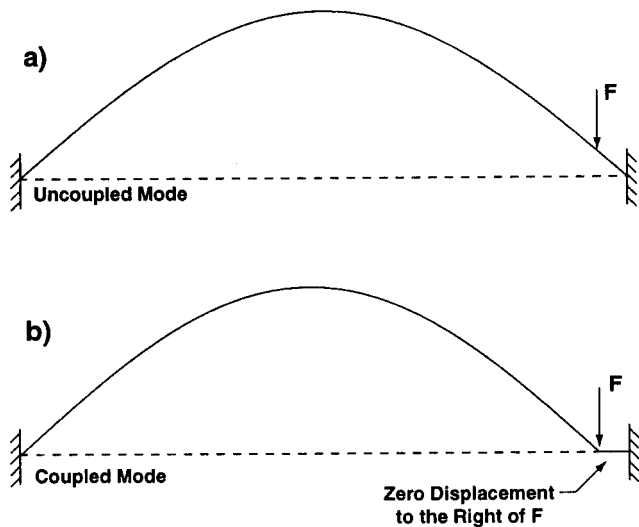


FIG. 5. Two different *first mode* vibration patterns. The first is the traditional first mode. The second has a dead zone to the right of the applied force and is caused by string-shaker coupling.

mm). Experimental results are given by the  $\times$  symbols while the linear and perturbation results are given by the solid lines in Figs. 4(a) and (b), respectively. For this small separation size, where linear motion is expected to dominate, both analytical techniques render good predictions below resonance. As the frequency approaches  $\Omega=1$ , the force required to cause impact decreases because of the amplitude amplification associated with resonance. Above resonance (say, above  $\Omega=1.1$ ), neither predicts impact accurately. This loss of consistency occurs because of shaker-string coupling in the experimental system. This coupling produced another weak resonance; it's mode shape has a node at the point of applications of the force and zero deflection to the right. This is sketched in Fig. 5(b). However, this mode is not resonant in the typical sense. There was not a peak in the amplitude as

the frequency was changed. Rather, it's amplitude stayed roughly constant over a range of frequencies ( $1.1 \leq \Omega \leq 1.5$ ).

For a slightly larger gap size,  $\bar{\sigma}=0.005$  ( $\sigma=3$  mm), the parameter diagrams are shown in Figs. 4(c) and (d). The linear analysis [Fig. 4(c)] predicts that the minimum required force level occurs at the linear resonance  $\Omega=1$ . But the minimum for the experimental results occurs at a higher frequency and at a higher force level. This may be explained as follows: the larger gap separation suggests that larger (non-linear) oscillations must take place for impact to occur. The hardening characteristics of the string system imply that more force will be required to reach this amplitude (since the system has stiffened) and that the maximum amplitude is achieved above the linear resonance (see Fig. 6 in the next section). The perturbation results [Fig. 4(d)] clearly demonstrate these trends, as the minimum has shifted up and to the right of  $\Omega=1$ . As with the small gap separation tests, agreement between theory and experiments breaks down at higher frequencies as the weak shaker-string coupled resonance begins to take effect.

## VI. RESPONSE CHARACTERISTICS

### A. Vibrations in the absence of the amplitude restraint

In the absence of the amplitude restraint, the system returns to the classic nonlinear string. Figure 6 shows both the experimental and analytical amplitude versus frequency response diagram for the string, under an excitation amplitude of 1 N. The  $\circ$  ( $+$ ) symbols indicate an increasing (decreasing) frequency sweep. The solid lines were generated using the perturbation solution. The experiments and analysis show reasonable qualitative and quantitative agreement. In terms of their qualitative trends, both clearly show that the response diagram bends to the right of the traditional linear (upright) response diagram, indicating a hardening system.

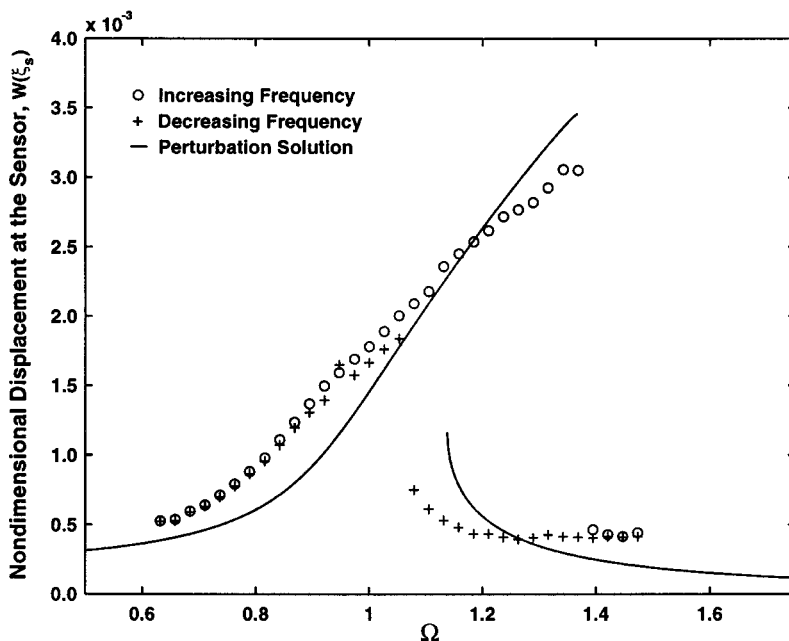


FIG. 6. The amplitude versus excitation frequency response diagram in the absence of impacts. Results from the experiment and the perturbation analysis are shown.

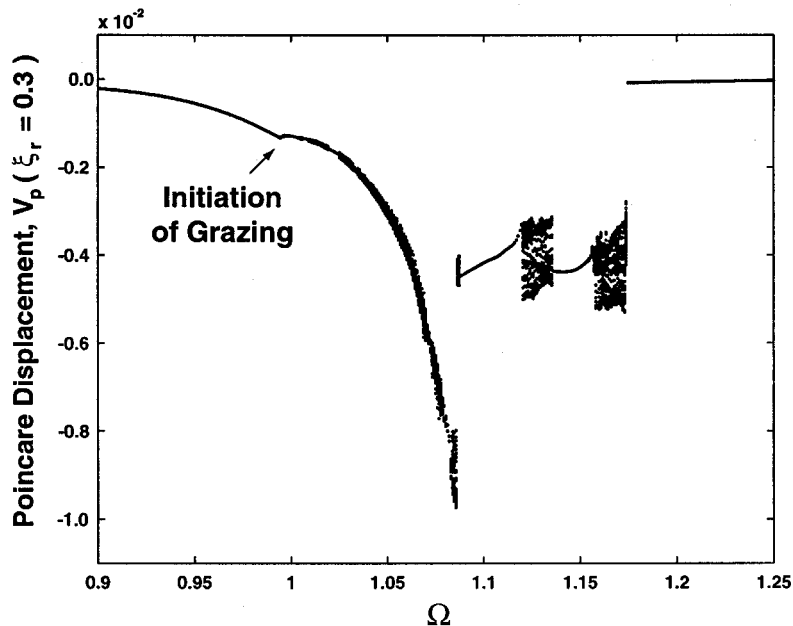


FIG. 7. A numerically generated amplitude versus excitation frequency response diagram, which includes impacts. Note the apparently chaotic portions as well as the periodic windows in the response.

Furthermore, both demonstrate an obvious dynamic hysteresis region, in which multiple periodic solutions coexist. Quantitatively, the amplitudes are close together over a range of frequencies. Also, the bifurcation frequencies, which produce the jump-in-amplitude, show reasonable agreement—though agreement is better for the jump down than for the jump up.

## B. Impacting response behavior

The remainder of the results presented here are based purely on the numerical simulation of the equation of motion. Although attempts were made to obtain experimental results, it became impossible to maintain a constant force amplitude due to the coupling between the string and the shaker. This coupling distorted the shape and amplitude of the input force wave form, and became stronger as the response grew and became less periodic. Hence, any agreement between the theoretical and experimental results would have been mere coincidence.

Figure 7 shows the steady-state string response as a function of the nondimensional excitation frequency. The response is taken at  $\xi = \xi_r = 0.3$  and is Poincaré sampled (once per forcing period) at zero phase relative to the excitation. At a frequency ratio of  $\Omega = 0.9$  the string is not contacting the knife edge and it is undergoing a period-one response. As the frequency ratio is increased, grazing occurs at  $\Omega = 0.9936$ . Immediately thereafter, the response ceases to be a simple, single frequency period-one oscillation. Higher period motion and chaos ensue (as will be discussed, shortly). However, several period-one windows emerge, notably in the ranges  $1.088 < \Omega < 1.12$  and  $1.1360 < \Omega < 1.155$ . At still higher frequencies, the response jumps down to a simple periodic motion.

Figure 8 shows some of the individual responses depicted in the response diagram. Figures 8(a), (b), and (c) correspond to  $\Omega = 0.9936$ , which is the grazing frequency where impacts are initiated. The time response is shown in

Fig. 8(a) and appears to be a period one oscillation. Figure 8(b) shows the associated velocity versus displacement trajectory (the pseudo-phase plane) for 40 orbits. This diagram, more than any other, clearly demonstrates the idea of grazing. The trajectory *grazes* the amplitude restraint [at  $V(\xi_r) = \bar{\sigma} = 5 \times 10^{-3}$ ] with zero velocity before moving away. The associated power spectrum is shown in Fig. 8(c) and indicates that this response is dominated by a single frequency.

Figures 8(d), (e), and (f) give the response at  $\xi_r$  inside one of the periodic windows:  $\Omega = 1.10037$ . In Figs. 8(d) and (e), the displacement never exceeds  $\bar{\sigma} = 0.005$ , as required by the stiff impact condition. Again, 40 cycles are shown in Fig. 8(e), demonstrating the complicated, yet periodic, character of the response. The power spectrum indicates that this periodic impacting motion has many frequencies participating.

Finally, Figs. 8(g), (h), and (i) show a nonperiodic response at  $\Omega = 1.12487$ . While the gross motion of Fig. 8(g) looks somewhat periodic, Fig. 8(h) clearly shows that the motion is nonperiodic. The power spectrum of this response, Fig. 8(i), has the broadband characteristics commonly associated with chaos.

One hallmark of a chaotic oscillation is that the phase space experiences both folding and stretching—giving the attractor a fractal structure. This can be described by the exponential divergence of nearby trajectories over short times in the phase space. The exponential divergence accounts for the stretching of the attractor. The expression “for short times” implies that these trajectories do not wander off indefinitely, since the attractor must be bounded; this accounts for the folding. Hence, quantifying this divergence (or, alternately, convergence) is one of the few definitive tests for chaotic motion. This is done in terms of Lyapunov exponents.

The technique for computing the Lyapunov exponents is described briefly here. A more thorough discussion may be found in the papers by Wolf *et al.*<sup>14</sup> and Abarbanel.<sup>15</sup> To begin, the system is integrated to steady state using the full

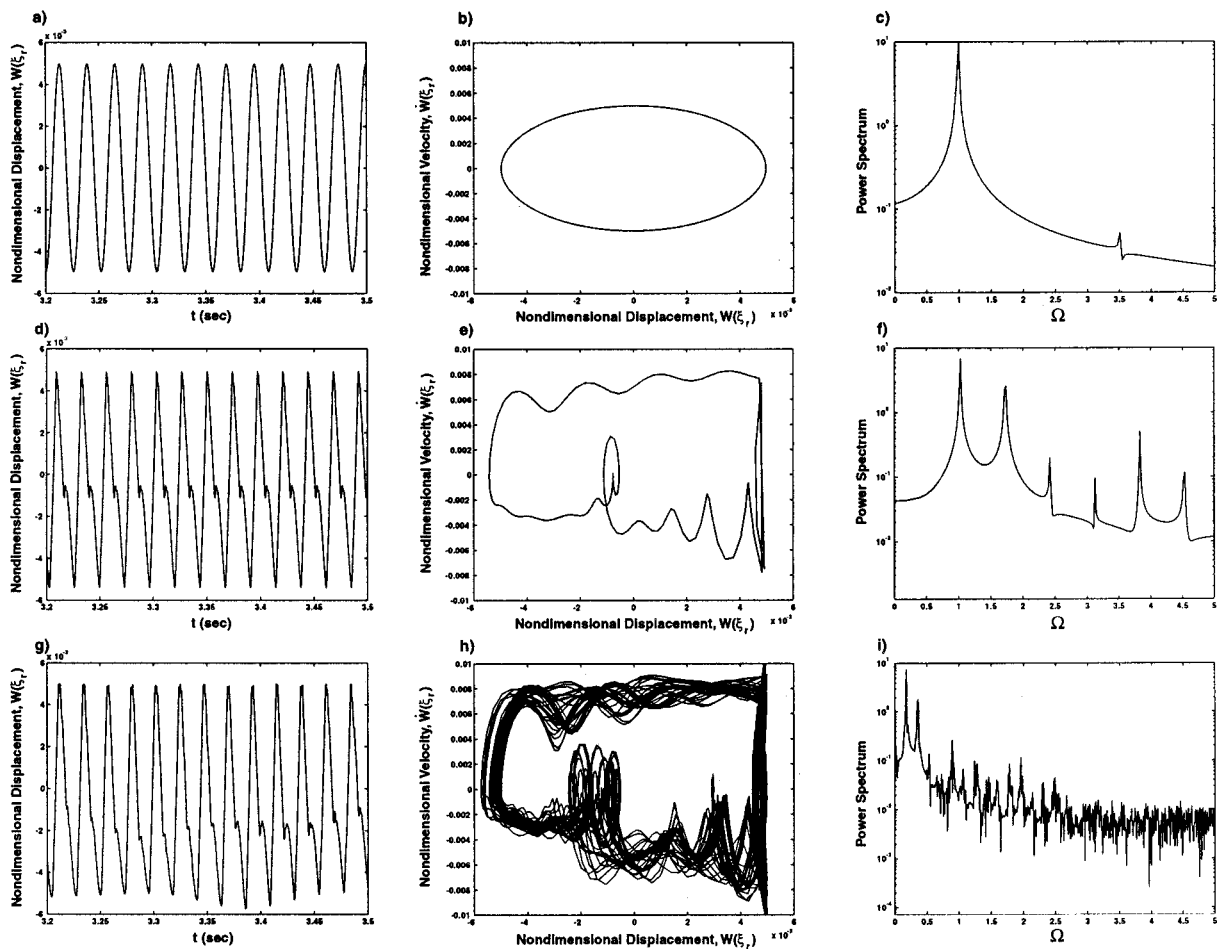


FIG. 8. Three numerical responses are shown. (a)–(c) Show the grazing response, where the trajectory impacts the restraint with zero velocity  $-\Omega=0.9936$ . (d)–(f) Is the response in one of the periodic windows,  $\Omega=1.0037$ . (g)–(i) Shows the aperiodic (chaotic) response,  $\Omega=1.12487$ .

nonlinear equations of motion, Eq. (8). Again, 20 modes have been incorporated, meaning that the phase space is 40 dimensional. Integration is temporarily stopped and the current time is defined as  $t_0$ . Forty initial conditions are prescribed  $\delta(t_0)$  away from the steady state solution—

along each of the phase space directions. This forms a 40-dimensional hypersphere, whose center is the actual trajectory of the string (dubbed the *fiducial* trajectory). Integration is resumed, with the fiducial trajectory being integrated with the full nonlinear equations. The equations governing the

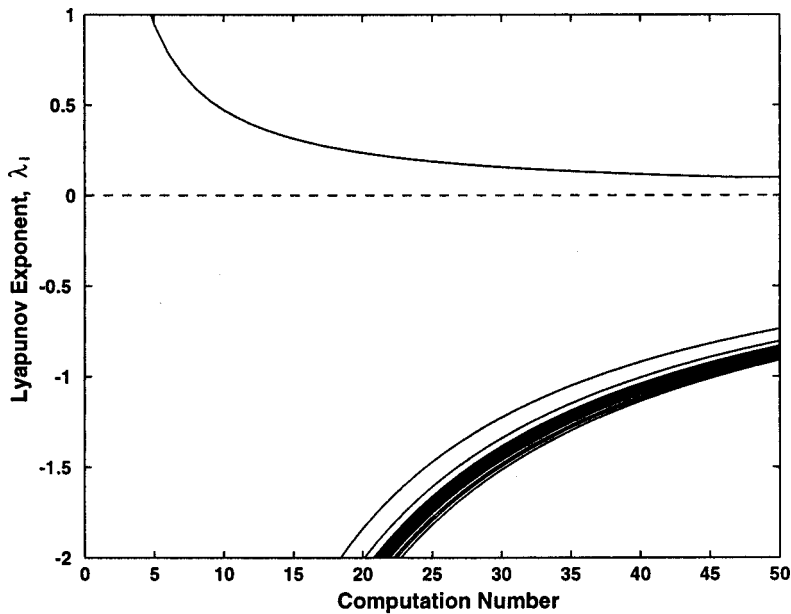


FIG. 9. The Lyapunov spectrum for the response at  $\Omega=1.12487$  [see Figs. 8(g)–(i)].

motion of the perturbed trajectories are linearized about the fiducial. As the sphere of initial conditions deforms under the action of the equations of motion, the relative stretching or compression of these axes may be computed by the formula

$$\lambda_i = \frac{1}{t-t_0} \ln \left( \frac{\delta_i(t)}{\delta(t_0)} \right). \quad (22)$$

These are the Lyapunov exponents for the motion. Of course, the exponents are calculated a number of times and averaged. This simply allows the results to be averaged over the attractor to give a more representative measure of the divergence.

The Lyapunov exponents have been calculated for the response  $\Omega = 1.12487$  [Figs. 8(g)–(i)] and are shown in Fig. 9. Here the 40 exponents are plotted as a function of the number of times the exponents are calculated. This figure shows that 39 are negative and one is positive with a value of 0.945. As a result, the aperiodic response is confirmed to be chaotic. But since only one exponent is positive and it is small, it is evident that the divergence is not very strong and the motion may be classified as weakly chaotic. This is consistent with the rather periodic looking response shown in Fig. 8(g).

## VII. CONCLUSIONS

This paper details some new results on the vibrations of a periodically excited string subject to an amplitude restraint. The amplitude restraint sets up an impacting condition, which provides a discontinuity in the stiffness. The principle focus of this work is to examine the grazing instability and the post-bifurcation response. First, this involves describing approximately the excitation parameter combinations ( $F, \Omega$ ) that lead to grazing. The response is then considered at a variety of excitation frequencies. It is shown that the grazing event leads to a nonperiodic response at higher frequencies, though periodic windows do appear in some frequency ranges. Typical responses are examined using its time re-

sponse, pseudo-phase plane projection, and the power spectrum. These responses ranged from the grazing incidence, to periodic impacts, to chaos. In the case of chaos, the response was confirmed by a Lyapunov exponent calculation. In all, these results shed light on some of the complicated response behavior that occurs in a periodically excited string subject to an amplitude restraint.

## ACKNOWLEDGMENTS

The support of the National Science Foundation (Grant No. CMS-9625319) is gratefully acknowledged.

- <sup>1</sup>F. Pfeiffer and A. Kunert, "Rattling models from deterministic to stochastic processes," *Nonlinear Dyn.* **1**, 63–74 (1990).
- <sup>2</sup>J. M. T. Thompson, "Complex dynamics of compliant off-shore structures," *Proc. R. Soc. London, Ser. A* **387**, 407–427 (1983).
- <sup>3</sup>P. V. Bayly and L. N. Virgin, "An experimental study of an impacting pendulum," *J. Sound Vib.* **164**, 364–374 (1993).
- <sup>4</sup>P. J. Holmes, "The dynamics of repeated impact with a sinusoidally vibrating table," *J. Sound Vib.* **84**, 173–189 (1982).
- <sup>5</sup>F. C. Moon and S. W. Shaw, "Chaotic vibrations of a beam with nonlinear boundary conditions," *Int. J. Non-Linear Mech.* **18**, 465–477 (1983).
- <sup>6</sup>S. W. Shaw, "Forced vibrations of a beam with one-sided amplitude constrain: theory and experiment," *J. Sound Vib.* **99**, 199–212 (1985).
- <sup>7</sup>T. Watanabe, "Forced vibrations of continuous system with non-linear boundary condition," *J. Mech. Des.* **100**, 487–491 (1978).
- <sup>8</sup>S. Foale and S. R. Bishop, "Bifurcations in impact oscillators: Theory and experiments," in *Nonlinearity and Chaos in Engineering Dynamics*, edited by J. M. T. Thompson and S. R. Bishop (Wiley, New York, 1994).
- <sup>9</sup>A. R. Champneys and P. J. McKenna, "On solitary waves of a piecewise linear suspended beam model," *Nonlinearity* **10**, 1763–1782 (1997).
- <sup>10</sup>C. Budd, F. Dux, and A. Cliffe, "The effect of frequency and clearance variations on single-degree-of-freedom impact oscillators," *J. Sound Vib.* **184**, 475–502 (1995).
- <sup>11</sup>A. B. Nordmark, "Non-periodic motion caused by grazing incidence on an impact oscillator," *J. Sound Vib.* **145**, 279–297 (1991).
- <sup>12</sup>R. Narasimha, "Nonlinear vibration of an elastic string," *J. Sound Vib.* **8**, 134–146 (1968).
- <sup>13</sup>M. Henon, "On the numerical computation of Poincaré maps," *Physica D* **5**, 412–414 (1982).
- <sup>14</sup>A. Wolf, J. B. Swift, H. L. Swinney, and J. A. Vastano, "Determining Lyapunov exponents from a time series," *Physica D* **16**, 285–317 (1985).
- <sup>15</sup>H. D. I. Abarbanel, "The analysis of observed chaotic data in physical systems," *Rev. Mod. Phys.* **65**, 1331–1390 (1993).